Cerebellum-Midbrain Reward Circuitry in Humans: an *in vivo* dissection

Linda J. Hoffman[1], *Josiah K. Leong*[2], *Holly Sullivan-Toole*[1], *Julia Foley*[1], *Blake L. Elliott*[1], *Ingrid R. Olson*[1]

[1]Temple University, Department of Psychology and Neuroscience, Philadelphia, PA, USA
[2]University of Arkansas, Department of Psychological Science, Fayetteville, AR, USA

Address correspondence to:

Linda J. Hoffman
Department of Psychology
Temple University
1701 N. 13th Street
Philadelphia, PA 19122

E-mail: linda.jasmine.hoffman@temple.edu
T: (215) 204-1708
F: (215) 204- 5539

Number of Key Points: 3
Word Count (Abstract): 198
Word Count (Body): 6192
References: 95
Number of Tables, Figures: 5, 3
Supplemental Tables, Figures: 12, 1
Keywords: cerebellum, midbrain, ventral tegmental area, diffusion imaging, addiction, obesity, reward

Abstract

Emerging research in non-human animals implicates cerebellar projections to the ventral tegmental area (VTA) in reward driven behaviors, but the circuits have not been characterized in humans. In this study we mapped the cerebello-VTA structural connectivity in humans. We visualized and measured the structural connections by performing probabilistic tractography on diffusion weighted imaging data from the Human Connectome Project (HCP). We uncovered the topographical organization of the connections by separately tracking from parcels of cerebellar lobule VI, crus I/II, vermis, paravermis, and cerebrocerebellum. The results revealed that afferents from the cerebellum to the VTA predominantly originate in the right hemisphere interposed nucleus and paravermis, and terminate mostly in ipsilateral VTA. The paravermis of the crus I cerebellar lobule sends the most connections to the VTA compared to the other lobules. Finally, we discovered a medial-to-lateral gradient of connectivity, such that medial cerebellum has the highest connectivity with the VTA, and connectivity decreases laterally. Taken together, we produced detailed maps of cerebello-VTA structural connectivity for the first time in humans. These maps provide critical foundation for future studies to investigate cerebellar involvement in social, affective, and reward-driven behaviors, as well as clinical manifestations at the extremes of those behaviors.

Key Points:

1. In humans, all cerebellar deep nuclei send projections to the VTA, which is similar to the connectivity profile found in non-human animals. The paravermis of Crus I contributes the most connections of the neocerebellum, and the interposed nucleus contributes the most connections among the deep nuclei.
2. There is a medial-to-lateral gradient of connectivity, such that more lateral segments of the cerebellum send fewer connections to the VTA.
3. These findings have implications for understanding normal and dysfunctional motivated behavior.

1. Introduction

The cerebellum is often overlooked by research on affective and motivated behaviors. While the principal outputs of the cerebellum project to the thalamus *en route* to the cerebral cortex, converging evidence across histology, axon tracing, and optogenetic research in non-human animals has established the existence of connections from the cerebellum to nearly every brainstem nucleus including those in the midbrain (Novello, Bosman, & De Zeeuw, 2022).

Purkinje cells are the sole output cells of the cerebellar cortex and they project to the three Deep Cerebellar Nuclei (DCN): the fastigial, interposed, and dentate nuclei (Purves, Augustine, & Fitzpatrick, 2001; Rajasekhar, 2022). A small number of studies have reported that the DCN project to the ventral tegmental area (VTA), a midbrain nucleus that plays a key role in motivated behavior as the origin of many dopaminergic cell bodies (Novello et al., 2022). Comparative research has established cerebello-VTA connections from axon tracer studies (Judd, Lewis, & Person, 2021; Perciavalle, Berretta, & Raffaele, 1989; Phillipson, 1979; R. S. Snider, Maiti, & Snider, 1976; Watabe-Uchida, Zhu, Ogawa, Vamanrao, & Uchida, 2012) in cats and rodents and optogenetic investigations in mice (Baek, Park, Kim, Yamamoto, & Tanaka-Yamamoto, 2022; Carta, Chen, Schott, Dorizan, & Khodakhah, 2019). Yet no research has characterized the cerebello-VTA structural connectivity in humans.

The importance of the cerebello-VTA pathway for motivated behavior is potentially quite profound. Carta and colleagues (2019) used optogenetics to transiently silence the DCN-VTA pathway in mice and found that stimuli that were usually rewarding—other mice—became uninteresting after the pathway was optogenetically inactivated. In a different study, Low and colleagues (2021) upregulated or downregulated a DCN-VTA pathway (from the lateral dentate) in mice and found that they could, respectively, increase or decrease the amount of food the mice ate, regardless of baseline satiety. Moreover, selectively activating or silencing these neurons could alter VTA activity such that more or less dopamine was released (Low et al., 2021). These findings suggest that portions of the cerebellum regulate reward signals that catalyze or inhibit reward-driven behavior, even without direct manipulation of central reward regions.

The cerebello-VTA pathway is potentially relevant to understanding the pathophysiology of diverse socio-affective disorders with disrupted reward-seeking behavior including disorders with prominent reductions in social motivation (e.g., social anxiety, schizophrenia, autism) (Berridge & Robinson, 2016), eating and substance use disorders (Berridge & Robinson, 2016; Morales & Berridge, 2020), and mood disorders (Pizzagalli, 2014). For example, the cerebello-VTA pathway may be important in disorders such as autism spectrum disorder, in which social reward processing is known to be disrupted (Dawson et al., 2004; Dawson, Webb, & McPartland, 2005; Han, Tomarken, & Gotham, 2019); unipolar depression, in which reduced reward responsivity is thought to be critical to the etiology and maintenance of the disorder (Pizzagalli, 2014; D. Watson & Naragon-Gainey, 2010), and bipolar disorder, which is hypothesized to be grounded in perturbed modulation of reward-seeking (Long et al., 2022; Loonen, Kupka, & Ivanova, 2017). All of these disorders have been variably linked to cerebellar dysfunction. For instance, studies using voxel based morphometry have reported changes in cerebellar thickness, density, or volume in individuals with bipolar disorder relative to healthy controls (Baldacara et al., 2011; DelBello, Strakowski, Zimmerman, Hawkins, & Sax, 1999; Eker et al., 2014; Kim et al., 2013; Lippmann et al., 1982; Lupo et al., 2021; Mills, Delbello, Adler, & Strakowski, 2005; Nasrallah, McCalley-Whitters, & Jacoby, 1982); but also see (Brambilla, Barale, Caverzasi, &

Soares, 2002; Laidi et al., 2015; Monkul et al., 2008). A recent study compared the incidence of psychiatric comorbidity following the onset of neurological disease between individuals with cerebellar pathology versus individuals with Parkinson's disease (Delle Chiaie et al., 2015). Results show that bipolar disorders were diagnosed in 31% of patients with cerebellar disease but none of the patients with Parkinson's disease, highlighting the potential importance of the cerebellum compared with the dopaminergic midbrain.

Here we asked the foundational question: does the cerebello-VTA pathway exist in humans? Once found, we asked a series of more granular questions: were the projections primarily ipsilateral or contralateral, and are they primarily from medial or lateral cerebellum? Based on our ongoing work on monetary and social rewards and the cerebellum (Popal, 2023) we restricted our analysis to cerebellar lobules VI, crus I and II. We chose these regions since they are among the largest, and also because they are the only regions in posterior lobe that have vermal regions corresponding to the neocerebellum, the phylogenetically newest portions of this structure (Amore et al., 2021). This careful dissection will set the foundation for understanding cerebello-VTA connectivity *in vivo*, as it is the first of its kind to be performed in humans. It is also the first of its kind to disentangle the relative contributions from sagittal segments from multiple cerebellar lobules to the VTA, to assess the density of connections coming from each of the DCN individually, and to interrogate the issue of laterality and directionality in cerebello-VTA connectivity.

2. Methods

2.1. Dataset

All imaging data was acquired from the minimally preprocessed S900 release of the Human Connectome Project dataset. For in-depth details concerning data acquisition parameters, preprocessing, and quality control for this dataset, see Van Essen and colleagues (Glasser et al., 2013; Marcus et al., 2013; Marcus et al., 2011; Sotiropoulos et al., 2013; Ugurbil et al., 2013; Van Essen et al., 2013; Van Essen et al., 2012).

2.2. Participant Selection

Our goal was to have a sample size of 100, evenly split between biological male and female participants, who varied in their raw Achenbach Adult Self-Report (ASR) depression and anxiety subscale scores. We did this so as to have sufficient variability on affectively relevant behavioral measures for planned follow-up investigations on individual differences in tract micro- and macrostructure in regard to emotion dysregulation. Candidate participants were eliminated from the dataset if they did not have diffusion-weighted scans or T1-weighted scans, were left-handed, or did not have complete ASR data. Once these factors were considered, an even number of males and females were chosen. The remaining participants were ranked according to their raw ASR depression and anxiety subscale scores. Men and women at the low, middle, and high end of the ASR subscale were randomly selected in a balanced manner until an equal number of men and women were acquired.

2.3. Regions of Interest

2.3.1. Cerebellar Regions & Sagittal Segmentation

All cerebellar ROIs were extracted from the Montreal Neurological Institute (MNI) probabilistic atlas for cerebellar lobules and deep nuclei (Diedrichsen, Balsters, Flavell, Cussans, & Ramnani, 2009; Diedrichsen et al., 2011) (see also https://www.diedrichsenlab.org/imaging/propatlas.htm). To prevent overlap with each other, deep nuclei, vermal, and lobule ROIs were thresholded at varying levels (see Table S1).

Zebrin-informed sagittal segmentation of bilateral cerebellar lobule VI and crus I and II was performed after setting the minimum threshold for each at 25 using the *fslmaths* command in FSL. This resulted in left and right regions for each lobule that were 20-voxels and 25-voxels wide, respectively. Each left and right lobule was then partitioned into 5-voxel segments along the x-axis, resulting in 4 segments per hemisphere for lobule VI, and 5 segments per hemisphere for crus I and II. Sagittal divisions are labeled by number, with higher numbers indicating more lateral portions of each lobule. For the purposes of the current analysis, segment 1 of the cerebellar lobules has been assigned the title of paravermis, or “spinocerebellum”, due to its medial positioning immediately adjacent to the vermis. Thus, segment 1 sends projections to the interposed nucleus (IN) in subsequent analyses. All other segments (i.e., 2 – 4 for lobule VI, and 2 – 5 for crus I and II) are considered part of the cerebrocerebellum, and therefore project to the dentate nucleus (DN).

Since the vermis contains subdivisions corresponding to each cerebellar lobule, and the particular portions of this structure that may be most important for social and affective functioning is still uncharted, for the sake of the current analysis we only investigate portions of the vermis that correspond to the cerebellar lobules of interest. Note that all vermal projections synapse onto the fastigial nucleus (FN) before leaving the cerebellum.

2.3.2. Brainstem Regions

Brainstem regions were extracted from the brainstem navigator atlas, derived from 7 Tesla (T) *in vivo* MRI using multiple contrasts and segmentation methods (https://www.nitrc.org/projects/brainstemnavig/) (Bianciardi et al., 2016). From this, we used the bilateral VTA as our target region in the brainstem. The red nucleus and inferior colliculus were also used from this atlas in the service of creating our exclusion masks, which is described in further detail below.

2.3.3. Transformations

To delineate these transformation parameters, a series of linear registrations were performed. First, subjects’ T1-weighted images were skull-stripped using FSL’s brain extraction tool, which executed a bias field and neck cleanup. Next, subjects’ topup-corrected, time-collapsed b0 images were registered to their respective T1-weighted anatomical images with six degrees of freedom and a correlation ratio cost function, yielding a diffusion to structural space conversion matrix. The same registration parameters were used to warp subjects’ T1-weighted images to the 2 x 2 x 2mm^3 MNI space brain template, creating a structural to standard space conversion file. Next, the inverse of the two aforementioned matrices was taken to produce a structural to diffusion space and a standard to structural space conversion matrix, respectively. Last, to acquire the diffusion to standard space transformation parameters, the structural to standard space and diffusion to structural space matrices were concatenated. Finally, the inverse of this file was taken to create the standard to diffusion space conversion matrix that was used to convert the spheres to subject space. This procedure was enacted in order to avoid performing transformations directly on images that transcend two different imaging modalities (i.e., T1-

weighted and diffusion MRI). Finally, the MNI to diffusion space transformation matrix was used in conjunction with FSL's non-linear registration tool, *fnirt*, to warp ROIs to diffusion space (Andersson, Jenkinson, & Smith, 2010).

2.5. Tractography

2.5.1. Exclusion Criteria

One of the key aims of the current investigation was to reveal monosynaptic, direct connections between the cerebellum and VTA. This is challenging due to the proximity of the VTA to the red nucleus and thalamus, which are waypoints in the cerebello-thalamo-cortical tract (CTC)—the largest cerebellar output tract (Palesi et al., 2015). Therefore, to show disociability between the cerebello-mesocephalic tract and the CTC, we excluded the thalamus and red nucleus bilaterally. To prevent overlap with the VTA, the VTA was subtracted from the red nucleus once in subject space, and the difference was used in the exclusion mask.

To ensure extraneous fibers were not reconstructed as part of this investigation, we also excluded the brainstem inferior to, and including the pons, the cerebellum contralateral to where each tractography was seeded, the VTA contralateral to that being targeted, and all lobes of the cerebral cortex. In the case of the decussating tract, we forced decussation at the level of the IC via the Wernekink commissure. To do this, we identified the last slice of the IC ROIs from the Brainstem Navigator atlas in MNI space and excluded all voxels superior to that slice in the hemisphere ipsilateral to the cerebellar seed region.

2.5.2. Multi-Shell, Multi-Tissue Constrained Spherical Deconvolutions

MRTrix3 (https://www.mrtrix.org/) was used to estimate voxel-wise response functions for each principal neural tissue compartment, including grey matter (GM), white matter (WM), and cerebral spinal fluid (CSF), using the *dhollander* algorithm (Dhollander, Mito, Raffelt, & Connelly, 2019; Dhollander, Raffelt, & Connelly, 2016, 2018). Multi-tissue orientation distribution functions (ODFs) for each macroscopic tissue type were then fit using the *msmt_csd* argument in the *dwi2fod* command. This approach capitalizing on the distinct diffusion properties of different tissue types, captured in multi-b-value, high angular resolution diffusion imaging (HARDI) sequence used in the Human Connectome Project dataset (Jeurissen, Tournier, Dhollander, Connelly, & Sijbers, 2014). Taking the multi-shell CSD approach allowed us to constrain tractography anatomically to neural white matter, yielding more precise reconstructions.

2.5.3. Tracking Parameters

Probabilistic tractography was performed using the iFOD2 algorithm in MRTrix3 using the *tckgen* command. Note that for all tractographies, streamline selection criteria were disabled.

All tractographies seeded in the cerebellar cortex were performed unidirectionally, with the VTA designated as both an inclusion and stopping criteria. In order to make conjectures about tract density, we seeded a fixed number of streamlines per voxel in the seed mask, with random placement of the seeds throughout. To control for differing seed size of distinct cerebellar cortical areas, we determined the lowest volumetric occurrence of any of the cortical seed regions within the cohort. We found the smallest size in any subject to be that of the vermis corresponding to right crus II, with a volume of 329 voxels. Using 5,000 seeding attempts per voxel as our default selection criteria, we calculated the total number of viable seeds for all lobule-based tractographies by multiplying 329 voxels by 5,000 seed attempts per voxels, resulting in 1,645,000 total seeds for each tractography. The seeding-attempts per voxel for all other lobule-based tractographies was anchored by the smallest volumetric occurrence for each seed in the cohort and was calculated by dividing the smallest seed volume for each tractography in our sample by 1,645,000 total seeds. This information is summarized in table S2.

For tractographies seeded in the DCN, tracking was performed unidirectionally, and bidirectionally. The latter was done in order to evaluate where each nucleus receives input from the cerebellar cortex on the way to the ventral tegmental area. Moreover, due to the small size of the DCN relative to the portions of cerebellar cortex under study, the total number of seeds was anchored at the smallest occurrence of any of the DCN. In this case, the smallest nucleus was found in a subject whose right fastigial nucleus was 91 voxels. Therefore, for all DCN tractographies, the total number of seeds was set at 91 voxels * 5,000 seeding attempts per voxel, yielding a total seed count of 455,000 for each tractography. The value of seeds per voxel for all other DCN-seeded tractographies was determined by dividing the smallest occurrence of each DCN in the cohort, divided by the total number of seeds (455,000). This information is summarized in table S2.

2.6. Macrostructural Indices

Subject-wise streamlines and tract length were extracted using the MrVista package (https://github.com/vistalab/vistasoft) in MATLAB version 2017b (9.3).

2.7. Statistical Analyses

All statistical analyses were performed in RStudio version 1.4.1717 (https://www.r-project.org/). Focused, pairwise contrasts were performed to ascertain the following comparisons pertaining to tract density: (1) contralaterally vs. ipsilaterally synapsing tracts, performed for each cerebellar segment; (2) right- versus left-traveling tracts; (3) vermal vs. paravermal, vermal vs. cerebrocerebellar, and paravermal vs. cerebrocerebellar tracts; (4) tracts originating in crus I vs. crus II, crus I vs. lobule VI, and crus II vs. lobule VI; (5) Projections to the VTA from the dentate nucleus vs. interposed nucleus, dentate nucleus vs. fastigial nucleus, and interposed nucleus vs. fastigial nucleus. All contrasts were performed using paired Wilcoxon signed-rank tests in the *rstatix* package. To get effect sizes, we used the *wilcox_effsize()* command. Moreover, we computed 95% percentile confidence intervals bootstrapped around the effect size using 10,000 iterations.

Note that the results for the polysynaptic circuitry are presented three different ways: (1) they are presented without any controls; (2) they are presented by controlling for the size of the DCN in each projection route. This is done by dividing the number of streamlines for each tract by the volume of the relevant DCN on a subject-wise basis; (3) they are presented while controlling for tract length, which is done by dividing the number of streamlines by tract length. In this way, DCN volume and tract length are treated as potential confounds, and the extent to which these three results converge is assessed in order to ascertain the relative importance of each in relation to our current findings.

For a visualization of the tractographies performed in the current analysis, see **Figure 1**.

Figure 1. Tractography results in a representative subject of connections from cerebellum to deep cerebellar nuclei to VTA. a. Right hemisphere ipsilaterally-traveling polysynaptic tracts are shown for sagittal segments (a, b, and $c_1 – c_4$) within each cerebellar lobule. b. Anatomical

Regions-Of-Interest (ROIs) include the 3 deep cerebellar nuclei (Fastigial, Interposed, and Dentate), and the VTA. Tractography results of the monosynaptic tracts between the deep cerebellar nuclei and VTA, color-coded by the nuclei from which they were seeded.

3. Results

Due to the large number of analyses in the current report, a narrative summary of the statistical results is provided below. To view detailed information on raw streamline analyses, including Bonferroni-corrected p-values, bootstrapped confidence intervals, effect sizes, and effect size magnitude summaries, please refer to **Tables 1-5**. For the success rate of all tractography reconstructions, please see **Table S3**. Finally, companion tables of length- and waypoint-corrected results can be found in supplemental information (**figure S1**, as well as **tables S4-S8** and **S9-S12**, respectively). In the following sections we present findings from the cerebellar cortex to the VTA (=polysynaptic tracts) and from the DCN to the VTA (=monosynaptic tracts).

Table 1. Nonparametric pairwise comparisons using Wilcoxon sign-rank test investigating streamline count differences based on tract direction, lobule, and segment. All confidence intervals were bootstrapped with 10,000 iterations. Directions are coded as follows: R-R = right to right (ipsilateral tract), L-L = left to left (ipsilateral tract), R-L = right to left (contralateral tract), L-R = left to right (contralateral tract). Segments are coded as follows: a = vermis, b = paravermis; $c_1 – c_4$ = neocerebellum, with higher numbers indicating more lateral segments. In instances where all instances of a tract were larger than its comparison tract, inferential statistics are not reported.

Polysynaptic Tractography											
Direction											
Measure 1	Measure 2	*n* 1	*n* 2	W	*p*	$p_{bonferroni}$		*Eff. Size*	CI 95%		Magnitude
									Lower	Upper	
R-R	L-L	92	80	551	2.37e-06	1.42e-05	****	.54	.37	.70	large
	R-L			33	4.10e-14	2.46e-13		.85	.82	.87	
	L-R		32								
L-L	R-L	80	80	2318	2.58e-09	1.55e-08	****	.71	.57	.81	large
	L-R		32	527	9.31e-10	5.59e-09		.87	.85	.87	
R-L				50	2.82e-05	1.69e-04	***	.70	.48	.85	
Lobule											
Measure 1	Measure 2	*n* 1	*n* 2	W	*p*	$p_{bonferroni}$		*Eff. Size*	CI 95%		Magnitude
									Lower	Upper	
Crus I	Crus II	49	56	508	.322	.966	ns	.16	.007	.44	small
	Lobule VI		43	391	.219	.657		.21	.01	.52	
Crus II		56		361	.669	> .999		.07	.005	.41	
Segment											
Measure 1	Measure 2	*n* 1	*n* 2	W	*p*	$p_{bonferroni}$		*Eff. Size*	CI 95%		Magnitude
									Lower	Upper	
a	b	77	83	1851.5	1.00e-03	1.50e-02	*	.39	.18	.58	moderate
	c_1		75	562	4.00e-03	5.60e-02	†	.37	.12	.60	
	c_2		62	217.5	8.70e-05	1.00e-03	**	.56	.33	.75	large
	c_3		48	27	1.83e-08	2.74e-07	****	.80	.66	.87	
	c_4		56	8	5.68e-12	8.52e-11		.86	.81	.87	
b	c_1	83	75	2443	1.93e-09	2.90e-08		.70	.56	.82	
	c_2		62	1701	7.49e-10	1.12e-08		.80	.71	.86	
	c_3		48	1125	7.11e-14	1.07e-12		.87	.85	.87	
	c_4		56	1431	2.46e-10	3.69e-09		.87	.87	.87	
c_1	c_2	75	62	1669.5	3.27e-09	4.90e-08		.77	.66	.84	
	c_3		48	1128	1.42e-14	2.13e-13		.87	.87	.87	
	c_4		56	1485	1.67e-10	2.50e-09					
c_2	c_3	62	48	990	1.14e-13	1.71e-12					
	c_4		56	1125	1.14-e09	1.71e-08					
c_3		48		946	2.27e-13	3.40e-12					

Table 2. Nonparametric pairwise comparisons using Wilcoxon sign-rank test investigating streamline count differences based on tract direction and deep nucleus. All confidence intervals were bootstrapped with 10,000 iterations. Directions are coded as follows: R-R = right to right (ipsilateral tract), L-L = left to left (ipsilateral tract), R-L = right to left (contralateral tract), L-R

= left to right (contralateral tract). FN=fastigial nucleus; IN=interposed nucleus; DN = dentate nucleus.

Monosynaptic Tractography											
Direction											
Measure 1	Measure 2	*n* 1	*n* 2	W	*p*	$p_{bonferroni}$		*Eff. Size*	CI 95%		Magnitude
									Lower	Upper	
R-R	L-L	101	100	4106	5.50e-08	3.30e-07	****	.54	.39	.68	large
	R-L		101	5080	2.20e-17	1.32e-16		.84	.81	.86	
	L-R		93	4371	5.66e-17	3.40e-16		.87	.87	.87	
L-L	R-L	100	101	4606	8.46e-13	5.08e-12		.72	.61	.80	
	L-R		93	4371	5.66e-17	3.40e-16		.87	.87	.87	
R-L		101		4075	4.56e-13	2.74e-12		.75	.65	.83	
Deep Cerebellar Nuclei											
Measure 1	Measure 2	*n* 1	*n* 2	W	*p*	$p_{bonferroni}$		*Eff. Size*	CI 95%		Magnitude
									Lower	Upper	
FN	IN	97	99	550	5.02e-11	1.51e-10	****	.67	.55	.77	large
	DN		94	2934	1.30e-02	3.90e-02	*	.26	.05	.46	small
IN		99		3943	1.67e-11	5.01e-11	****	.70	.57	.81	large

Table 3. Nonparametric pairwise comparisons using Wilcoxon signed-rank test investigating interactions between direction and lobule. All confidence intervals are bootstrapped using 10,000 iterations to yield stable estimates around the effect size.

Direction x Lobule											
Crus I											
Measure 1	Measure 2	*n* 1	*n* 2	W	*p*	$p_{bonferroni}$		*Eff. Size*	CI 95%		Magnitude
									Lower	Upper	
R-R	L-L	97	87	3131	1.97e-09	1.18e-08	****	.65	.51	.77	large
	R-L		90	3953	1.49e-15	8.94e-15		.85	.81	.86	
	L-R		52	1326	5.30e-10	3.18e-09		.87	.87	.87	
L-L	R-L	87	90	2818.5	5.04e-08	3.02e-07		.61	.45	.73	
	L-R		52	1325	5.63e-10	3.38e-09		.87	.86	.87	
R-L		90	52	1235.5	8.25e-08	4.95e-07		.75	.61	.85	
Crus II											
Measure 1	Measure 2	*n* 1	*n* 2	W	*p*	$p_{bonferroni}$		*Eff. Size*	CI 95%		Magnitude
									Lower	Upper	
R-R	L-L	99	90	3181	5.14e-06	3.08e-05	****	.48	.30	.64	moderate
	R-L		88	3856	2.90e-15	1.74e-14		.84	.80	.86	large
	L-R		60	1829	1.76e-11	1.06e-10		.87	.86	.87	
L-L	R-L	90	88	3019.5	1.12e-09	6.72e-09		.67	.55	.78	
	L-R		60	1828	1.85e-11	1.11e-10		.87	.86	.87	
R-L		88		1451	1.02e-07	6.12e-07		.71	.55	.83	
Lobule VI											
Measure 1	Measure 2	*n* 1	*n* 2	W	*p*	$p_{bonferroni}$		*Eff. Size*	CI 95%		Magnitude
									Lower	Upper	
R-R	L-L	95	86	2581.5	3.85e-04	2.00e-03	**	.39	.19	.57	moderate

	R-L		88	3873	1.64e-15	9.84e-15	****	.85	.82	.86	large
	L-R		45	990	1.14e-13	6.84e-13		.87	.87	.87	
L-L	R-L	86	88	3124	5.65e-12	3.39e-11		.77	.67	.83	
	L-R		45	989	2.27e-13	1.36e-12		.87	.86	.87	
R-L		88		810	1.63e-05	9.78e-05		.62	.40	.78	

Table 4. Nonparametric pairwise comparisons using Wilcoxon signed-rank test investigating interactions between direction and segment. All confidence intervals are bootstrapped using 10,000 iterations to yield stable estimates around the effect size.

Direction x Segment											
a											
Measure 1	Measure 2	*n* 1	*n* 2	W	*p*	$p_{bonferroni}$		*Eff. Size*	CI 95%		Magnitude
									Lower	Upper	
R-R	L-L	100	97	3695.5	5.87e-07	3.52e-06	****	.51	.34	.66	large
	R-L		98	4652	2.70e-16	1.62e-15		.83	.79	.86	
	L-R		78	3002	2.61e-14	1.57e-13		.87	.87	.87	
L-L	R-L	97	98	3478	2.66e-05	1.60e-04	***	.43	.25	.59	moderate
	L-R		78	3080	1.78e-14	1.07e-13	****	.87	.87	.87	large
R-L		98		2701.5	7.46e-09	4.48e-08		.65	.51	.78	
b											
Measure 1	Measure 2	*n* 1	*n* 2	W	*p*	$p_{bonferroni}$		*Eff. Size*	CI 95%		Magnitude
									Lower	Upper	
R-R	L-L	101	100	3637.5	1.32e-04	7.92e-04	***	.38	.20	.55	moderate
	R-L		98	4763	1.22e-16	7.32e-16	****	.84	.80	.86	large
	L-R		85	3655	1.19e-15	7.14e-15		.87	.87	.87	
L-L	R-L	100	98	4235.5	2.27e-11	1.36e-10		.68	.56	.77	
	L-R		85	3653	1.28e-15	7.68e-15		.87	.86	.87	
R-L		98		3144.5	2.01e-10	1.21e-09		.70	.57	.80	
c_1											
Measure 1	Measure 2	*n* 1	*n* 2	W	*p*	$p_{bonferroni}$		*Eff. Size*	CI 95%		Magnitude
									Lower	Upper	
R-R	L-L	99	94	3345	8.96e-06	5.38e-05	****	.46	.28	.63	moderate
	R-L		96	4615	6.51e-17	3.91e-16		.85	.83	.87	large
	L-R		76	2926	3.68e-14	2.21e-13		.87	.87	.87	
L-L	R-L	94	96	3379	3.62e-07	2.17e-06		.53	.37	.66	
	L-R		76	2925	3.83e-14	2.30e-13		.87	.87	.87	
R-L		96		2594	8.19e-11	4.91e-10		.75	.64	.84	
c_2											
Measure 1	Measure 2	*n* 1	*n* 2	W	*p*	$p_{bonferroni}$		*Eff. Size*	CI 95%		Magnitude
									Lower	Upper	
R-R	L-L	99	91	3348.5	3.69e-08	2.21e-07	****	.58	.42	.72	large
	R-L		92	4236	3.25e-16	1.95e-15		.85	.82	.87	
	L-R		64	2079	3.79e-12	2.27e-11		.87	.86	.87	
L-L	R-L	91	92	2978.5	6.69e-06	4.01e-05		.48	.30	.63	moderate
	L-R		64	2077	4.16e-12	2.50e-11		.87	.86	.87	large
R-L		92		1823	3.00e-09	1.80e-08		.75	.62	.85	
c_3											

Measure 1	Measure 2	n 1	n 2	W	p	$p_{bonferroni}$		*Eff. Size*	CI 95%		Magnitude
									Lower	Upper	
R-R	L-L	98	87	3072.5	2.30e-07	1.38e-06	****	.56	.38	.71	large
	R-L		91	4059	5.89e-16	3.53e-15		.85	.83	.87	
	L-R		50	1224	1.22e-09	7.32e-09		.87	.86	.87	
L-L	R-L	87	91	2694	4.52e-06	2.71e-05		.51	.33	.66	
	L-R		50	1222	1.78e-14	1.07e-13		.87	.85	.87	
R-L		91		1100.5	1.24e-06	7.44e-06		.69	.51	.83	

c_4

Measure 1	Measure 2	n 1	n 2	W	p	$p_{bonferroni}$		*Eff. Size*	CI 95%		Magnitude
									Upper	Lower	
R-R	L-L	97	88	2580	9.84e-04	6.00e-03	**	.36	.16	.54	moderate
	R-L			3794.5	1.76e-15	1.06e-14	****	.85	.82	.87	large
	L-R		59	1705	4.92e-11	2.95e-10		.86	.84	.87	
L-L	R-L	88	88	2545	9.23e-06	5.54e-05		.50	.31	.65	moderate
	L-R		59	1767	2.86e-11	1.72e-10		.87	.86	.87	large
R-L				1336.5	3.21e-07	1.93e-06		.69	.53	.81	

Table 5. Nonparametric pairwise comparisons using Wilcoxon signed-rank test investigating interactions between lobule and segment. All confidence intervals are bootstrapped using 10,000 iterations to yield stable estimates around the effect size.

Lobule x Segment

a

Measure 1	Measure 2	n 1	n 2	W	p	$p_{bonferroni}$		*Eff. Size*	CI 95%		Magnitude
									Lower	Upper	
Crus I	Crus II	80	90	491.5	4.97e-07	1.49e-06	****	.57	.40	.73	large
	Lobule VI		98	81	1.59e-13	4.77e-13		.83	.76	.87	
Crus II		90		483.5	5.21e-10	1.56e-09		.66	.52	.77	

b

Measure 1	Measure 2	n 1	n 2	W	p	$p_{bonferroni}$		*Eff. Size*	CI 95%		Magnitude
									Lower	Upper	
Crus I	Crus II	91	94	2994	1.64e-05	4.92e-05	****	.46	.28	.61	moderate
	Lobule VI		89	2744	5.98e-05	1.79e-04	***	.44	.24	.61	
Crus II		94		1749	6.02e-01	> .999	ns	.06	.004	.26	small

c_1

Measure 1	Measure 2	n 1	n 2	W	p	$p_{bonferroni}$		*Eff. Size*	CI 95%		Magnitude
									Lower	Upper	
Crus I	Crus II	94	89	2294.5	6.80e-02	2.05e-01	ns	.20	.02	.39	small
	Lobule VI		77	2482.5	1.32e-07	3.96e-07	****	.61	.43	.75	large
Crus II		89		1964.5	4.00e-03	1.30e-02	*	.33	.11	.54	moderate

c_2

Measure 1	Measure 2	n 1	n 2	W	p	$p_{bonferroni}$		*Eff. Size*	CI 95%		Magnitude
									Lower	Upper	
Crus I	Crus II	83	87	963	3.00e-03	8.00e-03	**	.34	0.13	0.53	moderate
	Lobule VI		64	2016	5.29e-12	1.59e-11	****	.87	0.87	0.87	large
Crus II		87		1952	8.15e-12	2.45e-11		.87	0.86	0.87	

c_3

Measure 1	Measure 2	*n* 1	*n* 2	W	*p*	$p_{bonferroni}$		*Eff. Size*	CI 95%		Magnitude
									Lower	Upper	
Crus I	Crus II	77	77	530	3.09e-05	9.27e-05	****	.50	.31	.67	moderate
	Lobule VI		50	1176	1.68e-09	5.04e-09		.87	.87	.87	large
Crus II				1275	7.77e-10	2.33e-09		.87	.87	.87	
c_4											
Measure 1	Measure 2	*n* 1	*n* 2	W	*p*	$p_{bonferroni}$		*Eff. Size*	CI 95%		Magnitude
									Lower	Upper	
Crus I	Crus II	64	69	710	.475	-	ns	.10	.006	.36	small

3.1. Main Effects

Polysynaptic tracts

First, focused Wilcoxon signed-rank tests revealed a main effect of direction such that more streamlines travel from the cerebellar cortex to the ipsilateral VTA. All possible direction combinations were significantly different from one another. There was an effect of laterality such that there was stronger connectivity from the right cerebellum to the VTA. This holds for both the ipsilaterally and contralateral (e.g., decussating) tract. This effect persists after controlling for DCN volume and tract length.

Second, pairwise comparisons revealed no main effect of lobule. This finding held when controlling for average tract length. However, when controlling for DCN volume as a confound, we found a significant difference in connectivity between lobule VI and crus I, as well as a trending difference (after Bonferroni correction) between lobule VI and crus II. Both effects are of moderate magnitude and suggest higher streamline density coming from lobule VI as compared to crus I/II.

Third, there is a main effect of “segment” such that nearly all segments significantly differ from one another. Pairwise comparisons between every segment revealed a higher number of streamlines coming from the paravermis (segment b) compared to the vermis proper. From there, there is a medial to lateral gradient of decreasing connectivity. However, when controlling for average tract length as a potential confound, the difference between the vermis (a) and paravermis (b) becomes non-significant, and the difference between the vermis and c_1 becomes significant such that the vermis has more connectivity to the VTA overall, while all other comparisons remain effectively unchanged. Finally, after controlling for DCN volume, the difference in direction between the vermis (a) and paravermis (b) flips, such that the vermally-seeded tracts contain higher streamline density travelling through the fastigial nucleus than does the paravermally-seeded tracts travelling through the interposed nucleus. Moreover, when controlling for DCN size, the difference between the vermis and c_1 remains significant. All other findings remain unchanged when controlling for DCN waypoint volume, meaning that the gradient of lessening connectivity with more laterally positioned segments endures.

Monosynaptic tracts

Focused Wilcoxon signed-rank tests revealed a main effect of direction such that more streamlines travel from the DCN to the ipsilateral VTA. All possible direction combinations were significantly different from one another. There was an effect of laterality such that there was stronger connectivity from the right DCN to the VTA. This holds for both the ipsilaterally and contralateral (e.g., decussating) tract. This effect persists after controlling for tract length.

Second, there is a main effect of DCN. Pairwise comparisons revealed that most streamlines going to the VTA come from the interposed nucleus, second most from the fastigial, and the least coming from the dentate. This effect was not confounded by tract length.

All findings concerning main effects are summarized in **Figure 2**.

Figure 2. A summary of statistical results investigating gross pairwise comparisons for both the polysynaptic (A) and monosynaptic (B) reconstructions. Each result is illustrated twice: on the left are the results using raw streamlines, and on the right are the streamline results when controlling for waypoint volume in voxels. The results for the lobule by segment interactions are illustrated by cerebellar flat maps in section (C). The flat map on the left is meant to orient the viewer to the location of the cerebellar lobules and segments under study, while the flat map on the right has highlighted on the lobule for each segment where streamline density was the highest. Note that segment c_1 is highlighted in crus I and II as both of these lobules contained more streamlines in this segment than lobule VI without being statistically different form each other. Also, segment c_4 contains no remaining highlights since the streamline count in crus I and II did not significantly differ from each other in this segment (not this segment did not extend into lobule VI).

3.2. Interactions

For the polysynaptic tractographies, there was neither an interaction between lobule and direction, nor between segment and direction. That is to say that regardless of lobule or segment being seeded, the ipsilaterally traveling tract always contained more streamlines to the VTA than the contralaterally traveling tract, and the tract seeded in the right cerebellum always contained more VTA connectivity than those seeded in the left. These findings are robust and persist when controlling for both length and waypoint volume in the case of the polysynaptic reconstructions.

There were, however, interactions between segment and lobule, such that different segments showed differing levels of connectivity between the three lobules under study. This is important because it provides insights into which lobule provides the most connectivity to the VTA within each segment. These findings are detailed below and in **Figure 3**. Findings for length and waypoint-controlled lobule by segment comparisons are summarized in **Supplemental Figure 1B**.

Figure 3. Topographical organization of cerebellum-VTA connectivity. a. Medial segments of each cerebellar lobule have the highest connectivity with the VTA. b. Representative tractography reconstructions for the segment of each cerebellar lobule with the highest connectivity to the VTA. Note that the laterality and directionality of the tracts are not meaningful, but show instances of decussation the polysynaptic reconstructions.

3.2.1. Vermis (Segment a)

All possible lobule comparisons were significantly different from each other in the vermis, such that crus I vermal connectivity to the VTA contained the lowest connectivity, while lobule VI contained the most. This interaction holds after controlling for both average tract length and waypoint volume. This means that within the vermal regions under study, lobule VI contains the highest contribution of connections to the VTA, a finding that holds after holding multiple confounds constant.

3.2.2. Paravermis (Segment b)

There was a significant difference between paravermal connectivity to the VTA originating in crus I such that the majority of connectivity from this segment originated in this lobule as compared to crus II and lobule VI. Furthermore, there was no difference between the relative amount of paravermal connectivity coming from crus II and lobule VI. This finding held when controlling for volume of the DCN waypoints. However, when controlling for average streamline length, only crus I and crus II remained significantly different from one another, with this difference remaining in the same direction.

3.2.3. Cerebrocerebellum Segment c_1

There was an interaction between lobule and segment in the case of c_1, such that lobule VI contains less VTA projections than both crus I and crus II while the latter two lobules remain non-significantly different from each other. This effect persists when controlling for waypoint volume. However, when controlling for length, it emerges that crus I contains more VTA connectivity than crus II and lobule VI, while the difference between crus II and lobule VI becomes non-significant.

3.2.4. Cerebrocerebellum Segments c_2 & c_3

All possible lobule comparisons in segment c_2 and c_3 were significantly different from one another, such that crus II contains the most VTA connectivity in these segments, while lobule VI contains the least. These effects held after controlling for average tract length and waypoint volume within these segments.

3.2.5. Cerebrocerebellum Segment c_4

There was no difference in segment c_4 between crus I/II, and one did not emerge when controlling for average tract length or waypoint volume.

4. Discussion

4.1. Current findings

In this study, we mapped the structural connectivity between the cerebellum and VTA for the first time in humans. Using diffusion weighted imaging and probabilistic tractography, we found robust structural connectivity between both cerebellar cortex and the VTA, as well as cerebellar nuclei and the VTA. We then examined these connections at a higher level of granularity which revealed the following findings. First, connections are most robust in the ipsilateral direction, although contralateral connections do exist. Second, there is higher tract density from the right cerebellum/right DCN to the VTA as compared to the left cerebellum/left DCN, suggest some lateralization of function. Third, when we segmented crus I, II, and lobule IV, we found that there was a medial to lateral gradient such that the highest connectivity to the VTA was from the paravermis (segment b), with decreasing tract density as you moved lateral. Likewise, when we examined the monosynaptic tracts from the DCN to the VTA, the greatest density was from the interposed, followed by the fastigial, then the dentate nucleus.

4.2. The deep cerebellar nuclei, their inputs, and their outputs

The fastigial (or medial) nucleus is the smallest and most medial of the DCN. Just lateral to it is the interposed nucleus (or Latin '*nucleus interpositus*'), and lateral to that is the largest nucleus, the dentate (or lateral) nucleus (Schmahmann, 2019). This orderly array of nuclei receives their input from the cerebellum in a spatially orderly way. The fastigial nucleus receives it's input from the most medial region of the cerebellum, the vermis. The interposed nucleus receives its input from the region just lateral to the vermis, the paravermis, while the dentate receives its input from all the other regions in the cerebellum (Apps et al., 2018; Perciavalle et al., 2013; Voogd & Glickstein, 1998).

In our study, we found the highest density of streamlines from the cerebellum to the VTA was from the paravermis, and predictably, from the interposed nucleus. The interposed nucleus output runs through the ipsilateral superior cerebellar peduncle and decussates at the ponto-mesencephalic junction. Prior histology findings have reported that these pathways go to the red nucleus, ventral lateral nucleus of the thalamus, periaqueductal grey, the superior colliculus (Nieuwenhuys, Voogd, & Huijzen, 2008), and the VTA (Novello et al., 2022). Very little is known about this nucleus, though certain conjectures regarding its function may be gleaned from analyzing the role of the paravermis from which it receives its afferent connections. While the paravermis is known to calibrate motor control of the distal limbs (Unverdi & Alsayouri, 2023), other studies are slowly expanding the role of this region, beyond motor calibration. Paravermal lesions in mice result in downstream spikes in dopamine D1 receptor (DRD1) activity in the contralateral medial striatum, and dopamine transporter (DAT) attenuation in the dorsolateral striatum (Delis, Mitsacos, & Giompres, 2013). The influence of the interposed nucleus and the paravermis on dopamine activity is echoed in an antecedent study by S. R. Snider and Snider (1979), who found that paravermal lesions exert chronic effects on forebrain dopamine concentrations. This is interesting in light of our current findings due to the fact that DRD1 activity is implicated in a number of psychiatric conditions, as well as in social interest (Homberg et al., 2016).

The second highest density of streamlines was from the fastigial nucleus. The fastigial nucleus has a known role in our ability to stand and move about the world without falling over or becoming nauseous from conflicting sensory signals. With input from the vermis, it orchestrates the complex signals required for rapid postural changes, which includes not only muscular adjustments, but also changes in heart rate, blood pressure, and eye movements (Stiedl, Youn, & Jansen, 2010; Sullivan, Rose, & Pfefferbaum, 2006; Takagi, Zee, & Tamargo, 1998). However new evidence is expanding our ideas of what this nucleus may perform. It appears to play a role in motivated behavior such as aggressive and defensive behavior as well as eating. Studies in rodents have found direct connections between the fastigial and periaqueductal gray, amygdala, hippocampus, septal nuclei, and hypothalamus (Cao et al., 2013; Fujita, Kodama, & du Lac, 2020; Heath & Harper, 1974; R. S. Snider & Maiti, 1976; Zhang, Wang, & Zhu, 2016). Lesions in the rat cerebellar vermis (which projects to the fastigial) decreased innate fear, seen by an increase in approach behavior in the cat test and enhancement of motor activity in the open field test (Supple, Leaton, & Fanselow, 1987). In addition, more recent evidence suggests that it is involved in feeding because stimulation of these neurons can modulate initiation or cessation of feeding (Li, Guo, Tang, Zhu, & Wang, 2009). There are also implications regarding the fastigial nucleus as it pertains to rodent models of schizophrenia, as stimulation of this region begot alterations in medial prefrontal dopamine activity, which tends to be disrupted in this disorder (Hadley et al., 2014; Parker, Narayanan, & Andreasen, 2014; T. C. Watson, Jones, & Apps, 2009).

In the current study, the most robust VTA-projecting region of the neocerebellar vermis came from lobule VI. Functional imaging studies of the cerebellum suggest several related possibilities for lobule VI of the vermis: that it is involved in saccadic eye movements, motor planning, bilateral hand movements, divided attention, visual working memory, and reconciliation of conflicting input (King, Hernandez-Castillo, Poldrack, Ivry, & Diedrichsen, 2019). Given the highly motoric nature of this vermal region, lobule VI white matter projections to the VTA may work in concert with this structure in the service of motivated behavior. This idea is bolstered by recent rodent work revealing that GABAergic neurons in the VTA are involved in head movements in the appetitive pursuit of a moving target (Hughes et al., 2019; Masullo & Tripodi, 2019). It is possible then that the vermal portion of the cerebello-VTA tract may coordinate hedonic seeking behavior – the intersection of movement and reward - by way of the fastigial nucleus.

Finally, the least robust cerebello-VTA connections in our study were from the largest nucleus in the cerebellum, the dentate nucleus. The dorsal dentate consists of motor projections while the ventral dentate consists of projections to association cortices involved in cognitive and sensory processes (Bernard et al., 2014; Dimitrova et al., 2006; Dum & Strick, 2003; Palesi et al., 2015; Steele et al., 2017; Thurling et al., 2012). Around half of the dentate nucleus volume is involved in nonmotor domains (Palesi et al., 2021). Bauer, Kerr, and Swain (2011) performed dentate nuclei lesions in rats, and found that they exhibited decreased hedonic motivation, hallmarks of certain psychiatric disorders. Low et al. (2021) upregulated or downregulated a lateral dentate-VTA pathway in mice and found that they could increase or decrease the amount of food the mice ate, regardless of baseline satiety and the effect was linked to dopamine levels. Carta et al. (2019) showing that integrity of the dentate-VTA pathway in mice was necessary for social preference behavior in a three-chamber social task. A more recent study conducted by Baek et al. (2022) revealed that crus I Purkinje cells in mice, by way of the dentate nucleus, influence VTA activity. Furthermore, this study showed that deactivation of VTA-projecting dentate neurons attenuated depression symptoms as evaluated by performance on the open-field test, tail suspension test, and forced swimming test. Conversely, this report showed that long-term excitation of this circuit exacerbated depression-like symptoms in stressed mice.

We would like to emphasize that our findings showed that all three deep nuclei project to the VTA, which is consistent with histology findings. For instance, one viral tracing study in mice revealed projections between the interposed nucleus and the VTA (Judd et al., 2021). Another tracing study in rats that used horseradish peroxidase (HRP) injections into the VTA found retrograde labels in both the contralateral dentate and interposed nuclei. The same procedure was repeated in an anterograde fashion, with results showing that tracer injections in the dentate and interposed nuclei both traveled to the contralateral VTA (Perciavalle et al., 1989). Yet another study found that the fastigial nucleus in the cat and rat contain ipsilateral projections to the VTA by way of the accessory brachium conjunctivum (also known as the superior cerebellar peduncle) (R. S. Snider et al., 1976). Moreover, the interposed and dentate nuclei were found to connect to the contralateral VTA in these animals (R. S. Snider et al., 1976). Taken together, findings from non-human animal work using a variety of techniques provide support for cerebello-VTA connectivity, both ipsilateral and contralateral, from all three DCN (Novello et al., 2022). Our research extends these anatomic findings to humans.

Projections from each DCN nuclei target different regions of the VTA (Yoshida et al., 2022). Future research will need to disentangle the potentially distinct contributions of each DCN-VTA pathway to behavior.

4.3. How these fiber paths might relate to neuropsychiatric disorders

There is a robust literature linking a range of neuropsychiatric disorders (e.g., depression, schizophrenia, addiction, eating disorders, and ADHD) to aberrance in the dopamine system (Blum et al., 2008; Schmidt et al., 2001; Yu, Miller, & Groth, 2022). There is a separate literature linking various neuropsychiatric disorders (e.g., autism spectrum disorder, schizophrenia, unipolar depression, bipolar depression, substance abuse) to perturbations in the cerebellum. We previously reviewed the literature on cerebellar lesions and mood disorders and found that the incidence of unipolar and bipolar depression increased tremendously following cerebellar injury (Frazier et al., 2022). For instance, Delle Chiaie et al. (2015) found that the incidence of mood disorders was unusually high amongst those with cerebellar lesions, compared to those with Parkinson's disease. Further evidence bolstering the role of the cerebellum in the pathophysiology of mood disorders comes from Kim et al. (2013), who identified a 30% prevalence rate of depression in those having sustained cerebellar strokes—a proportion more than three times larger than that measured in the general population. Moreover, other cerebellar lesion studies have uncovered symptoms ranging from flattened affect, lassitude, and aberrant peripheral physiological markers of emotion processing (Annoni, Ptak, Caldara-Schnetzer, Khateb, & Pollermann, 2003). Our study lays the ground for understanding how the diverse anatomy of cerebellar connectivity can manifest neuropsychiatric dysfunctions.

4.4. Relationship to other white matter tracts

The cerebello-VTA pathway described in this study may correspond, at least in part to the trunk of the medial forebrain bundle (MFB), which in one study, extended as far back as the ipsilateral dentate nucleus of the human cerebellum (Coenen, Panksepp, Hurwitz, Urbach, & Madler, 2012). A better understanding of the trunk of the MFB will be needed to advance our etiological understanding of the social and affective deficits emanating from cerebellar lesions (Frazier et al., 2022). It is also the critical to enhance our understanding of this tract as it is an effective site for deep-brain stimulation (DBS) interventions for depression (Coenen et al., 2019; Conner, Quevedo, Soares, & Fenoy, 2022).

It is also possible that the cerebello-VTA pathway is a distinct pathway, that links to the MFB, through its cerebrocerebellar segments. However, it is yet unknown if the MFB contains afferents originating in the more medial DCN. Additionally, it is unclear if the identified projections map onto other larger white matter bundles, or if they are in isolation their own entity.

4.5. Limitations

One limitation of the current report is that we only investigated cerebellar afferents to the VTA. That is, we did not investigate connections originating in the VTA and synapsing onto the DCN and cerebellar cortex—connections whose existence are supported by the rodent literature but have yet to be charted in humans (Ikai, Takada, Shinonaga, & Mizuno, 1992). This disadvantage is compounded by the fact that it precludes us from investigating cerebellar innervation patterns within the VTA itself. Related to this, we only investigated three cerebellar lobules in the posterior lobe and corresponding portions of the vermis. Future investigators should examine the connectivity between the anterior lobe, as well as lobules VIIB-X in the posterior lobe, to the VTA.

Another limitation is the current report’s reliance on streamlines as the macrostructural index of interest, as it is known to be confounded by length, curvature, and branching, and may not correspond to tract density per se (Hoffman et al., 2022; Jones, Knosche, & Turner, 2013; Zhang et al., 2016). The number of streamlines reconstructed using DWI methods may not correspond to the actual number of axonal projections comprising the tract in question. Finally, probabilistic tracking algorithms such as the one employed in this study can be prone to false positive reconstructions (Maier-Hein et al., 2017). We hope that future investigators corroborate our findings using *ex vivo* techniques which do not suffer from these limitations.

4.6. Conclusions and future directions

Future research should disentangle where the cerebellum sends projections after the VTA. One possibility is the bed nucleus of the stria terminalis (BNST)—a small grey matter region in the extended amygdala known to be sensitive to stress and to exhibit large sex differences (Phillipson, 1979). Several tracer studies support this relationship (Baek et al., 2022; Watabe-Uchida et al., 2012). Understanding this circuitry may provide insight into the complex relationship between stress and motivated behavior. In addition, the interconnectedness of the cerebellum, VTA, and hypothalamus should be explored to investigate how cerebellar modulation of VTA signals to regions involved in appetitive functioning may inform aberrant feeding behaviors in humans. Additionally, future research should investigate if there is a dissociation between the socio-emotional behaviors underpinned by VTA connections to each DCN, and if higher-ordered social functions are subserved by cerebrocerebellar inputs to the VTA from the dentate.

As the field of cognitive neuroscience turns its attention to the cerebellum to understand the pathophysiology of socio-affective disorders implicated by optogenetic studies manipulating cerebellar connections to the VTA, it will be necessary to know where in the human cerebellum to look for the most robust projections. Building off the cat and rodent literature describing cerebello-VTA projections (Novello et al., 2022), this study is the first in humans to provide a field map for cerebello-VTA connectivity, delineating where investigators are most likely to find the dopabello tract. This will be useful for *in vivo* brain-behavior investigations not only as researchers turn to which deep nuclei project most strongly to the VTA, but where in the cerebellar cortex these projections originate. The current report suggests that the vermis and paravermis, along with the most medial portions of the cerebrocerebellum are most likely to provide input to the VTA, and that these connections are most likely to originate in the right cerebellum and travel ipsilaterally. Moreover, amongst regions of the neocerebellum, vermal (i.e., segment a) lobule VI, paravermal (i.e., segment b) crus I, and the medial cerebrocerebellar (i.e., segment c_1) crus I/II, are where one may begin to look in any investigation of the socio-affective correlates of cerebello-VTA white matter. In this way, this study sets the stage for a more cohesive human brain mapping of the cerebello-dopaminergic system, and follow-up investigations of its behavioral correlates.

Acknowledgements: We would like to thank Drs. Volker Coenen, Marco Reisert, and Sascha du Lac, for their insights into cerebello-midbrain connectivity and insights into the cerebellar afferents to each deep cerebellar nucleus, respectively. Moreover, we would like to thank Katie Jobson for her contributions pertaining to our understanding of the CTC. Finally, we would also like to thank Haroon Popal and Vishnu Murty for contributing their knowledge on reward circuitry.

Conflicts of interest: Authors report no conflict of interest.

Funding sources: This research includes calculations carried out on HPC resources supported in part by the National Science Foundation through major research instrumentation grant number 1625061 and by the US Army Research Laboratory under contract number W911NF-16-2-0189. This work was supported by a National Institute of Health grants to I. Olson (R21 HD098509; R01 NICHD R01HD099165; R56 MH091113; R01 MH118545-01A1) and to H. Sullivan-Toole (F32 MH127948-01A1). The content is solely the responsibility of the authors and does not necessarily represent the official views of the National Institute of Mental Health or the National Institutes of Health. The authors declare no competing financial interests.

References:

Amore, G., Spoto, G., Ieni, A., Vetri, L., Quatrosi, G., Di Rosa, G., & Nicotera, A. G. (2021). A Focus on the Cerebellum: From Embryogenesis to an Age-Related Clinical Perspective. *Front Syst Neurosci, 15*, 646052. doi:10.3389/fnsys.2021.646052

Andersson, J. L. R., Jenkinson, M., & Smith, S. (2010). *Non-linear registration, aka spatial normalisation*. Retrieved from

Annoni, J. M., Ptak, R., Caldara-Schnetzer, A. S., Khateb, A., & Pollermann, B. Z. (2003). Decoupling of autonomic and cognitive emotional reactions after cerebellar stroke. *Ann Neurol, 53*(5), 654-658. doi:10.1002/ana.10549

Apps, R., Hawkes, R., Aoki, S., Bengtsson, F., Brown, A. M., Chen, G., . . . Ruigrok, T. J. H. (2018). Cerebellar Modules and Their Role as Operational Cerebellar Processing Units: A Consensus paper [corrected]. *Cerebellum, 17*(5), 654-682. doi:10.1007/s12311-018-0952-3

Baek, S. J., Park, J. S., Kim, J., Yamamoto, Y., & Tanaka-Yamamoto, K. (2022). VTA-projecting cerebellar neurons mediate stress-dependent depression-like behaviors. *Elife, 11*. doi:10.7554/eLife.72981

Baldacara, L., Nery-Fernandes, F., Rocha, M., Quarantini, L. C., Rocha, G. G., Guimaraes, J. L., . . . Jackowski, A. (2011). Is cerebellar volume related to bipolar disorder? *J Affect Disord, 135*(1-3), 305-309. doi:10.1016/j.jad.2011.06.059

Bauer, D. J., Kerr, A. L., & Swain, R. A. (2011). Cerebellar dentate nuclei lesions reduce motivation in appetitive operant conditioning and open field exploration. *Neurobiol Learn Mem, 95*(2), 166-175. doi:10.1016/j.nlm.2010.12.009

Bernard, J. A., Peltier, S. J., Benson, B. L., Wiggins, J. L., Jaeggi, S. M., Buschkuehl, M., . . . Seidler, R. D. (2014). Dissociable functional networks of the human dentate nucleus. *Cereb Cortex, 24*(8), 2151-2159. doi:10.1093/cercor/bht065

Berridge, K. C., & Robinson, T. E. (2016). Liking, wanting, and the incentive-sensitization theory of addiction. *Am Psychol, 71*(8), 670-679. doi:10.1037/amp0000059

Bianciardi, M., Toschi, N., Eichner, C., Polimeni, J. R., Setsompop, K., Brown, E. N., . . . Wald, L. L. (2016). In vivo functional connectome of human brainstem nuclei of the ascending arousal, autonomic, and motor systems by high spatial resolution 7-Tesla fMRI. *MAGMA, 29*(3), 451-462. doi:10.1007/s10334-016-0546-3

Blum, K., Chen, A. L., Braverman, E. R., Comings, D. E., Chen, T. J., Arcuri, V., . . . Oscar-Berman, M. (2008). Attention-deficit-hyperactivity disorder and reward deficiency syndrome. *Neuropsychiatr Dis Treat, 4*(5), 893-918. doi:10.2147/ndt.s2627

Brambilla, P., Barale, F., Caverzasi, E., & Soares, J. C. (2002). Anatomical MRI findings in mood and anxiety disorders. *Epidemiol Psichiatr Soc, 11*(2), 88-99. doi:10.1017/s1121189x00005558

Cao, B. B., Huang, Y., Lu, J. H., Xu, F. F., Qiu, Y. H., & Peng, Y. P. (2013). Cerebellar fastigial nuclear GABAergic projections to the hypothalamus modulate immune function. *Brain Behav Immun, 27*(1), 80-90. doi:10.1016/j.bbi.2012.09.014

Carta, I., Chen, C. H., Schott, A. L., Dorizan, S., & Khodakhah, K. (2019). Cerebellar modulation of the reward circuitry and social behavior. *Science, 363*(6424). doi:10.1126/science.aav0581

Coenen, V. A., Bewernick, B. H., Kayser, S., Kilian, H., Bostrom, J., Greschus, S., . . . Schlaepfer, T. E. (2019). Superolateral medial forebrain bundle deep brain stimulation in major depression: a gateway trial. *Neuropsychopharmacology, 44*(7), 1224-1232. doi:10.1038/s41386-019-0369-9

Coenen, V. A., Panksepp, J., Hurwitz, T. A., Urbach, H., & Madler, B. (2012). Human medial forebrain bundle (MFB) and anterior thalamic radiation (ATR): imaging of two major subcortical pathways and the dynamic balance of opposite affects in understanding depression. *J Neuropsychiatry Clin Neurosci, 24*(2), 223-236. doi:10.1176/appi.neuropsych.11080180

Conner, C. R., Quevedo, J., Soares, J. C., & Fenoy, A. J. (2022). Brain metabolic changes and clinical response to superolateral medial forebrain bundle deep brain stimulation for treatment-resistant depression. *Mol Psychiatry, 27*(11), 4561-4567. doi:10.1038/s41380-022-01726-0

Dawson, G., Toth, K., Abbott, R., Osterling, J., Munson, J., Estes, A., & Liaw, J. (2004). Early social attention impairments in autism: social orienting, joint attention, and attention to distress. *Dev Psychol, 40*(2), 271-283. doi:10.1037/0012-1649.40.2.271

Dawson, G., Webb, S. J., & McPartland, J. (2005). Understanding the nature of face processing impairment in autism: insights from behavioral and electrophysiological studies. *Dev Neuropsychol, 27*(3), 403-424. doi:10.1207/s15326942dn2703_6

DelBello, M. P., Strakowski, S. M., Zimmerman, M. E., Hawkins, J. M., & Sax, K. W. (1999). MRI analysis of the cerebellum in bipolar disorder: a pilot study. *Neuropsychopharmacology, 21*(1), 63-68. doi:10.1016/S0893-133X(99)00026-3

Delis, F., Mitsacos, A., & Giompres, P. (2013). Lesion of the cerebellar paravermis increases dopamine D1 receptor levels in the contralateral striatum. *J Chem Neuroanat, 47*, 35-41. doi:10.1016/j.jchemneu.2012.10.004

Delle Chiaie, R., Minichino, A., Salviati, M., Fiorentini, S., Tonini, A., Bersani, F. S., . . . Biondi, M. (2015). Bipolar Spectrum Disorders in Patients With Cerebellar Lesions: A Comparison With Parkinson's Disease. *J Nerv Ment Dis, 203*(9), 725-729. doi:10.1097/NMD.0000000000000359

Dhollander, T., Mito, R., Raffelt, D., & Connelly, A. (2019). *Improved white matter response function estimation for 3-tissue constrained spherical deconvolution*. Paper presented at the 27th International Society of Magnetic Resonance in Medicine, Montréal, Québec, Canada.

Dhollander, T., Raffelt, D., & Connelly, A. (2016). *Unsupervised 3-tissue response function estimation from single-shell or multi-shell diffusion MR data without a co-registered T1 image*. Paper presented at the ISMRM Workshop on Breaking the Barriers of Diffusion MRI, Lisbon, Portugal.

Dhollander, T., Raffelt, D., & Connelly, A. (2018). *Accuracy of response function estimation algorithms for 3-tissue spherical deconvolution of diverse quality diffusion MRI data*. Paper presented at the Society of Magnetic Resonance in Medicine, Paris, France.

Diedrichsen, J., Balsters, J. H., Flavell, J., Cussans, E., & Ramnani, N. (2009). A probabilistic MR atlas of the human cerebellum. *Neuroimage, 46*(1), 39-46. doi:10.1016/j.neuroimage.2009.01.045

Diedrichsen, J., Maderwald, S., Kuper, M., Thurling, M., Rabe, K., Gizewski, E. R., . . . Timmann, D. (2011). Imaging the deep cerebellar nuclei: a probabilistic atlas and normalization procedure. *Neuroimage, 54*(3), 1786-1794. doi:10.1016/j.neuroimage.2010.10.035

Dimitrova, A., de Greiff, A., Schoch, B., Gerwig, M., Frings, M., Gizewski, E. R., & Timmann, D. (2006). Activation of cerebellar nuclei comparing finger, foot and tongue movements as revealed by fMRI. *Brain Res Bull, 71*(1-3), 233-241. doi:10.1016/j.brainresbull.2006.09.015

Dum, R. P., & Strick, P. L. (2003). An unfolded map of the cerebellar dentate nucleus and its projections to the cerebral cortex. *J Neurophysiol, 89*(1), 634-639. doi:10.1152/jn.00626.2002

Eker, C., Simsek, F., Yilmazer, E. E., Kitis, O., Cinar, C., Eker, O. D., . . . Gonul, A. S. (2014). Brain regions associated with risk and resistance for bipolar I disorder: a voxel-based MRI study of patients with bipolar disorder and their healthy siblings. *Bipolar Disord, 16*(3), 249-261. doi:10.1111/bdi.12181

Frazier, M. R., Hoffman, L. J., Popal, H., Sullivan-Toole, H., Olino, T. M., & Olson, I. R. (2022). A missing link in affect regulation: the cerebellum. *Soc Cogn Affect Neurosci, 17*(12), 1068-1081. doi:10.1093/scan/nsac042

Fujita, H., Kodama, T., & du Lac, S. (2020). Modular output circuits of the fastigial nucleus for diverse motor and nonmotor functions of the cerebellar vermis. *Elife, 9*. doi:10.7554/eLife.58613

Glasser, M. F., Sotiropoulos, S. N., Wilson, J. A., Coalson, T. S., Fischl, B., Andersson, J. L., . . . Consortium, W. U.-M. H. (2013). The minimal preprocessing pipelines for the Human Connectome Project. *Neuroimage, 80*, 105-124. doi:10.1016/j.neuroimage.2013.04.127

Hadley, J. A., Nenert, R., Kraguljac, N. V., Bolding, M. S., White, D. M., Skidmore, F. M., . . . Lahti, A. C. (2014). Ventral tegmental area/midbrain functional connectivity and response to antipsychotic medication in schizophrenia. *Neuropsychopharmacology, 39*(4), 1020-1030. doi:10.1038/npp.2013.305

Han, G. T., Tomarken, A. J., & Gotham, K. O. (2019). Social and nonsocial reward moderate the relation between autism symptoms and loneliness in adults with ASD, depression, and controls. *Autism Res, 12*(6), 884-896. doi:10.1002/aur.2088

Heath, R. G., & Harper, J. W. (1974). Ascending projections of the cerebellar fastigial nucleus to the hippocampus, amygdala, and other temporal lobe sites: evoked potential and histological studies in monkeys and cats. *Exp Neurol, 45*(2), 268-287. doi:10.1016/0014-4886(74)90118-6

Hoffman, L. J., Ngo, C. T., Canada, K. L., Pasternak, O., Zhang, F., Riggins, T., & Olson, I. R. (2022). The fornix supports episodic memory during childhood. *Cereb Cortex, 32*(23), 5388-5403. doi:10.1093/cercor/bhac022

Homberg, J. R., Olivier, J. D., VandenBroeke, M., Youn, J., Ellenbroek, A. K., Karel, P., . . . Ellenbroek, B. A. (2016). The role of the dopamine D1 receptor in social cognition: studies using a novel genetic rat model. *Dis Model Mech, 9*(10), 1147-1158. doi:10.1242/dmm.024752

Hughes, R. N., Watson, G. D. R., Petter, E. A., Kim, N., Bakhurin, K. I., & Yin, H. H. (2019). Precise Coordination of Three-Dimensional Rotational Kinematics by Ventral Tegmental Area GABAergic Neurons. *Curr Biol, 29*(19), 3244-3255 e3244. doi:10.1016/j.cub.2019.08.022

Ikai, Y., Takada, M., Shinonaga, Y., & Mizuno, N. (1992). Dopaminergic and non-dopaminergic neurons in the ventral tegmental area of the rat project, respectively, to the cerebellar cortex and deep cerebellar nuclei. *Neuroscience, 51*(3), 719-728. doi:10.1016/0306-4522(92)90310-x

Jeurissen, B., Tournier, J. D., Dhollander, T., Connelly, A., & Sijbers, J. (2014). Multi-tissue constrained spherical deconvolution for improved analysis of multi-shell diffusion MRI data. *Neuroimage, 103*, 411-426. doi:10.1016/j.neuroimage.2014.07.061

Jones, D. K., Knosche, T. R., & Turner, R. (2013). White matter integrity, fiber count, and other fallacies: the do's and don'ts of diffusion MRI. *Neuroimage, 73*, 239-254. doi:10.1016/j.neuroimage.2012.06.081

Judd, E. N., Lewis, S. M., & Person, A. L. (2021). Diverse inhibitory projections from the cerebellar interposed nucleus. *Elife, 10*. doi:10.7554/eLife.66231

Kim, D., Cho, H. B., Dager, S. R., Yurgelun-Todd, D. A., Yoon, S., Lee, J. H., . . . Lyoo, I. K. (2013). Posterior cerebellar vermal deficits in bipolar disorder. *J Affect Disord, 150*(2), 499-506. doi:10.1016/j.jad.2013.04.050

King, M., Hernandez-Castillo, C. R., Poldrack, R. A., Ivry, R. B., & Diedrichsen, J. (2019). Functional boundaries in the human cerebellum revealed by a multi-domain task battery. *Nat Neurosci, 22*(8), 1371-1378. doi:10.1038/s41593-019-0436-x

Laidi, C., d'Albis, M. A., Wessa, M., Linke, J., Phillips, M. L., Delavest, M., . . . Houenou, J. (2015). Cerebellar volume in schizophrenia and bipolar I disorder with and without psychotic features. *Acta Psychiatr Scand, 131*(3), 223-233. doi:10.1111/acps.12363

Li, B., Guo, C. L., Tang, J., Zhu, J. N., & Wang, J. J. (2009). Cerebellar fastigial nuclear inputs and peripheral feeding signals converge on neurons in the dorsomedial hypothalamic nucleus. *Neurosignals, 17*(2), 132-143. doi:10.1159/000197913

Lippmann, S., Manshadi, M., Baldwin, H., Drasin, G., Rice, J., & Alrajeh, S. (1982). Cerebellar vermis dimensions on computerized tomographic scans of schizophrenic and bipolar patients. *Am J Psychiatry, 139*(5), 667-668. doi:10.1176/ajp.139.5.667

Long, X., Wang, X., Tian, F., Cao, Y., Xie, H., & Jia, Z. (2022). Altered brain activation during reward anticipation in bipolar disorder. *Transl Psychiatry, 12*(1), 300. doi:10.1038/s41398-022-02075-w

Loonen, A. J. M., Kupka, R. W., & Ivanova, S. A. (2017). Circuits Regulating Pleasure and Happiness in Bipolar Disorder. *Front Neural Circuits, 11*, 35. doi:10.3389/fncir.2017.00035

Low, A. Y. T., Goldstein, N., Gaunt, J. R., Huang, K. P., Zainolabidin, N., Yip, A. K. K., . . . Betley, J. N. (2021). Reverse-translational identification of a cerebellar satiation network. *Nature, 600*(7888), 269-273. doi:10.1038/s41586-021-04143-5

Lupo, M., Olivito, G., Gragnani, A., Saettoni, M., Siciliano, L., Pancheri, C., . . . Leggio, M. (2021). Comparison of Cerebellar Grey Matter Alterations in Bipolar and Cerebellar Patients: Evidence from Voxel-Based Analysis. *Int J Mol Sci, 22*(7). doi:10.3390/ijms22073511

Maier-Hein, K. H., Neher, P. F., Houde, J. C., Cote, M. A., Garyfallidis, E., Zhong, J., . . . Descoteaux, M. (2017). The challenge of mapping the human connectome based on diffusion tractography. *Nat Commun, 8*(1), 1349. doi:10.1038/s41467-017-01285-x

Marcus, D. S., Harms, M. P., Snyder, A. Z., Jenkinson, M., Wilson, J. A., Glasser, M. F., . . . Consortium, W. U.-M. H. (2013). Human Connectome Project informatics: quality control, database services, and data visualization. *Neuroimage, 80*, 202-219. doi:10.1016/j.neuroimage.2013.05.077

Marcus, D. S., Harwell, J., Olsen, T., Hodge, M., Glasser, M. F., Prior, F., . . . Van Essen, D. C. (2011). Informatics and data mining tools and strategies for the human connectome project. *Front Neuroinform, 5*, 4. doi:10.3389/fninf.2011.00004

Masullo, L., & Tripodi, M. (2019). Goal-Oriented Behaviour: The Ventral Tegmental Area in Motivated Movements. *Curr Biol, 29*(19), R922-R925. doi:10.1016/j.cub.2019.08.041

Mills, N. P., Delbello, M. P., Adler, C. M., & Strakowski, S. M. (2005). MRI analysis of cerebellar vermal abnormalities in bipolar disorder. *Am J Psychiatry, 162*(8), 1530-1532. doi:10.1176/appi.ajp.162.8.1530

Monkul, E. S., Hatch, J. P., Sassi, R. B., Axelson, D., Brambilla, P., Nicoletti, M. A., . . . Soares, J. C. (2008). MRI study of the cerebellum in young bipolar patients. *Prog Neuropsychopharmacol Biol Psychiatry, 32*(3), 613-619. doi:10.1016/j.pnpbp.2007.09.016

Morales, I., & Berridge, K. C. (2020). 'Liking' and 'wanting' in eating and food reward: Brain mechanisms and clinical implications. *Physiol Behav, 227*, 113152. doi:10.1016/j.physbeh.2020.113152

Nasrallah, H. A., McCalley-Whitters, M., & Jacoby, C. G. (1982). Cerebral ventricular enlargement in young manic males. A controlled CT study. *J Affect Disord, 4*(1), 15-19. doi:10.1016/0165-0327(82)90014-3

Nieuwenhuys, R., Voogd, J., & Huijzen, C. (2008). *The Human Central Nervous System: A Synopsis and Atlas* (4 ed.): Steinkopff Heidelberg.

Novello, M., Bosman, L. W. J., & De Zeeuw, C. I. (2022). A Systematic Review of Direct Outputs from the Cerebellum to the Brainstem and Diencephalon in Mammals. *Cerebellum*. doi:10.1007/s12311-022-01499-w

Palesi, F., Ferrante, M., Gaviraghi, M., Misiti, A., Savini, G., Lascialfari, A., . . . Gandini Wheeler-Kingshott, C. A. M. (2021). Motor and higher-order functions topography of the human dentate nuclei identified with tractography and clustering methods. *Hum Brain Mapp, 42*(13), 4348-4361. doi:10.1002/hbm.25551

Palesi, F., Tournier, J. D., Calamante, F., Muhlert, N., Castellazzi, G., Chard, D., . . . Wheeler-Kingshott, C. A. (2015). Contralateral cerebello-thalamo-cortical pathways with prominent involvement of associative areas in humans in vivo. *Brain Struct Funct, 220*(6), 3369-3384. doi:10.1007/s00429-014-0861-2

Parker, K. L., Narayanan, N. S., & Andreasen, N. C. (2014). The therapeutic potential of the cerebellum in schizophrenia. *Front Syst Neurosci, 8*, 163. doi:10.3389/fnsys.2014.00163

Perciavalle, V., Apps, R., Bracha, V., Delgado-Garcia, J. M., Gibson, A. R., Leggio, M., . . . Sanchez-Campusano, R. (2013). Consensus paper: current views on the role of cerebellar interpositus nucleus in movement control and emotion. *Cerebellum, 12*(5), 738-757. doi:10.1007/s12311-013-0464-0

Perciavalle, V., Berretta, S., & Raffaele, R. (1989). Projections from the intracerebellar nuclei to the ventral midbrain tegmentum in the rat. *Neuroscience, 29*(1), 109-119. doi:10.1016/0306-4522(89)90336-9

Phillipson, O. T. (1979). Afferent projections to the ventral tegmental area of Tsai and interfascicular nucleus: a horseradish peroxidase study in the rat. *J Comp Neurol, 187*(1), 117-143. doi:10.1002/cne.901870108

Pizzagalli, D. A. (2014). Depression, stress, and anhedonia: toward a synthesis and integrated model. *Annu Rev Clin Psychol, 10*, 393-423. doi:10.1146/annurev-clinpsy-050212-185606

Popal, H. S. (2023). *Pinpointing the role of the cerebellum in social reward processing.* (Ph.D. Dissertation). Temple University,

Purves, D., Augustine, G. J., & Fitzpatrick, D. (2001). Circuits within the Cerebellum. In D. Purves, G. J. Augustine, & D. Fitzpatrick (Eds.), *Neuroscience* (2 ed.). Sunderland, MA: Sinauer Associates.

Rajasekhar, S. S. S. N. (2022). Anatomy of Cerebellum. In P. B. Ambrosi (Ed.), *Spinocerebellar Ataxia - Concepts, Particularities and Generalities*: IntechOpen.

Schmahmann, J. D. (2019). The cerebellum and cognition. *Neurosci Lett, 688*, 62-75. doi:10.1016/j.neulet.2018.07.005

Schmidt, K., Nolte-Zenker, B., Patzer, J., Bauer, M., Schmidt, L. G., & Heinz, A. (2001). Psychopathological correlates of reduced dopamine receptor sensitivity in depression, schizophrenia, and opiate and alcohol dependence. *Pharmacopsychiatry, 34*(2), 66-72. doi:10.1055/s-2001-15184

Snider, R. S., & Maiti, A. (1976). Cerebellar contributions to the Papez circuit. *J Neurosci Res, 2*(2), 133-146. doi:10.1002/jnr.490020204

Snider, R. S., Maiti, A., & Snider, S. R. (1976). Cerebellar pathways to ventral midbrain and nigra. *Exp Neurol, 53*(3), 714-728. doi:10.1016/0014-4886(76)90150-3

Snider, S. R., & Snider, R. S. (1979). Kainic acid: enduring alterations in cerebellar morphology and in cerebral catecholamine and GABA concentrations after cerebellar injection in the rat. *Neurosci Lett, 12*(2-3), 339-342. doi:10.1016/0304-3940(79)96086-5

Sotiropoulos, S. N., Jbabdi, S., Xu, J., Andersson, J. L., Moeller, S., Auerbach, E. J., . . . Consortium, W. U.-M. H. (2013). Advances in diffusion MRI acquisition and processing in the Human Connectome Project. *Neuroimage, 80*, 125-143. doi:10.1016/j.neuroimage.2013.05.057

Steele, C. J., Anwander, A., Bazin, P. L., Trampel, R., Schaefer, A., Turner, R., . . . Villringer, A. (2017). Human Cerebellar Sub-millimeter Diffusion Imaging Reveals the Motor and Non-motor Topography of the Dentate Nucleus. *Cereb Cortex, 27*(9), 4537-4548. doi:10.1093/cercor/bhw258

Stiedl, O., Youn, J. U., & Jansen, R. F. (2010). Cardiovascular conditioning: neural substrates. In G. Koob, R. F. Thompson, & M. Le Moal (Eds.), *Encyclopedia of Behavioral Neurosciences* (Vol. 1, pp. 226-235). Amsterdam: Elsevier.

Sullivan, E. V., Rose, J., & Pfefferbaum, A. (2006). Effect of vision, touch and stance on cerebellar vermian-related sway and tremor: a quantitative physiological and MRI study. *Cereb Cortex, 16*(8), 1077-1086. doi:10.1093/cercor/bhj048

Supple, W. F., Jr., Leaton, R. N., & Fanselow, M. S. (1987). Effects of cerebellar vermal lesions on species-specific fear responses, neophobia, and taste-aversion learning in rats. *Physiol Behav, 39*(5), 579-586. doi:10.1016/0031-9384(87)90156-9

Takagi, M., Zee, D. S., & Tamargo, R. J. (1998). Effects of lesions of the oculomotor vermis on eye movements in primate: saccades. *J Neurophysiol, 80*(4), 1911-1931. doi:10.1152/jn.1998.80.4.1911

Thurling, M., Hautzel, H., Kuper, M., Stefanescu, M. R., Maderwald, S., Ladd, M. E., & Timmann, D. (2012). Involvement of the cerebellar cortex and nuclei in verbal and visuospatial working memory: a 7 T fMRI study. *Neuroimage, 62*(3), 1537-1550. doi:10.1016/j.neuroimage.2012.05.037

Ugurbil, K., Xu, J., Auerbach, E. J., Moeller, S., Vu, A. T., Duarte-Carvajalino, J. M., . . . Consortium, W. U.-M. H. (2013). Pushing spatial and temporal resolution for functional and diffusion MRI in the Human Connectome Project. *Neuroimage, 80,* 80-104. doi:10.1016/j.neuroimage.2013.05.012

Unverdi, M., & Alsayouri, K. (2023). *Neuroanatomy, Cerebellar Dysfunction*. Retrieved from https://www.ncbi.nlm.nih.gov/books/NBK545251/

Van Essen, D. C., Smith, S. M., Barch, D. M., Behrens, T. E., Yacoub, E., Ugurbil, K., & Consortium, W. U.-M. H. (2013). The WU-Minn Human Connectome Project: an overview. *Neuroimage, 80*, 62-79. doi:10.1016/j.neuroimage.2013.05.041

Van Essen, D. C., Ugurbil, K., Auerbach, E., Barch, D., Behrens, T. E., Bucholz, R., . . . Consortium, W. U.-M. H. (2012). The Human Connectome Project: a data acquisition perspective. *Neuroimage*, *62*(4), 2222-2231. doi:10.1016/j.neuroimage.2012.02.018

Voogd, J., & Glickstein, M. (1998). The anatomy of the cerebellum. *Trends Neurosci, 21*(9), 370-375. doi:10.1016/s0166-2236(98)01318-6

Watabe-Uchida, M., Zhu, L., Ogawa, S. K., Vamanrao, A., & Uchida, N. (2012). Whole-brain mapping of direct inputs to midbrain dopamine neurons. *Neuron, 74*(5), 858-873. doi:10.1016/j.neuron.2012.03.017

Watson, D., & Naragon-Gainey, K. (2010). On the specificity of positive emotional dysfunction in psychopathology: evidence from the mood and anxiety disorders and schizophrenia/schizotypy. *Clin Psychol Rev, 30*(7), 839-848. doi:10.1016/j.cpr.2009.11.002

Watson, T. C., Jones, M. W., & Apps, R. (2009). Electrophysiological mapping of novel prefrontal - cerebellar pathways. *Front Integr Neurosci, 3*, 18. doi:10.3389/neuro.07.018.2009

Yoshida, J., Onate, M., Khatami, L., Vera, J., Nadim, F., & Khodakhah, K. (2022). Cerebellar Contributions to the Basal Ganglia Influence Motor Coordination, Reward Processing, and Movement Vigor. *J Neurosci, 42*(45), 8406-8415. doi:10.1523/JNEUROSCI.1535-22.2022

Yu, Y., Miller, R., & Groth, S. W. (2022). A literature review of dopamine in binge eating. *J Eat Disord, 10*(1), 11. doi:10.1186/s40337-022-00531-y

Zhang, X. Y., Wang, J. J., & Zhu, J. N. (2016). Cerebellar fastigial nucleus: from anatomic construction to physiological functions. *Cerebellum Ataxias, 3*, 9. doi:10.1186/s40673-016-0047-1

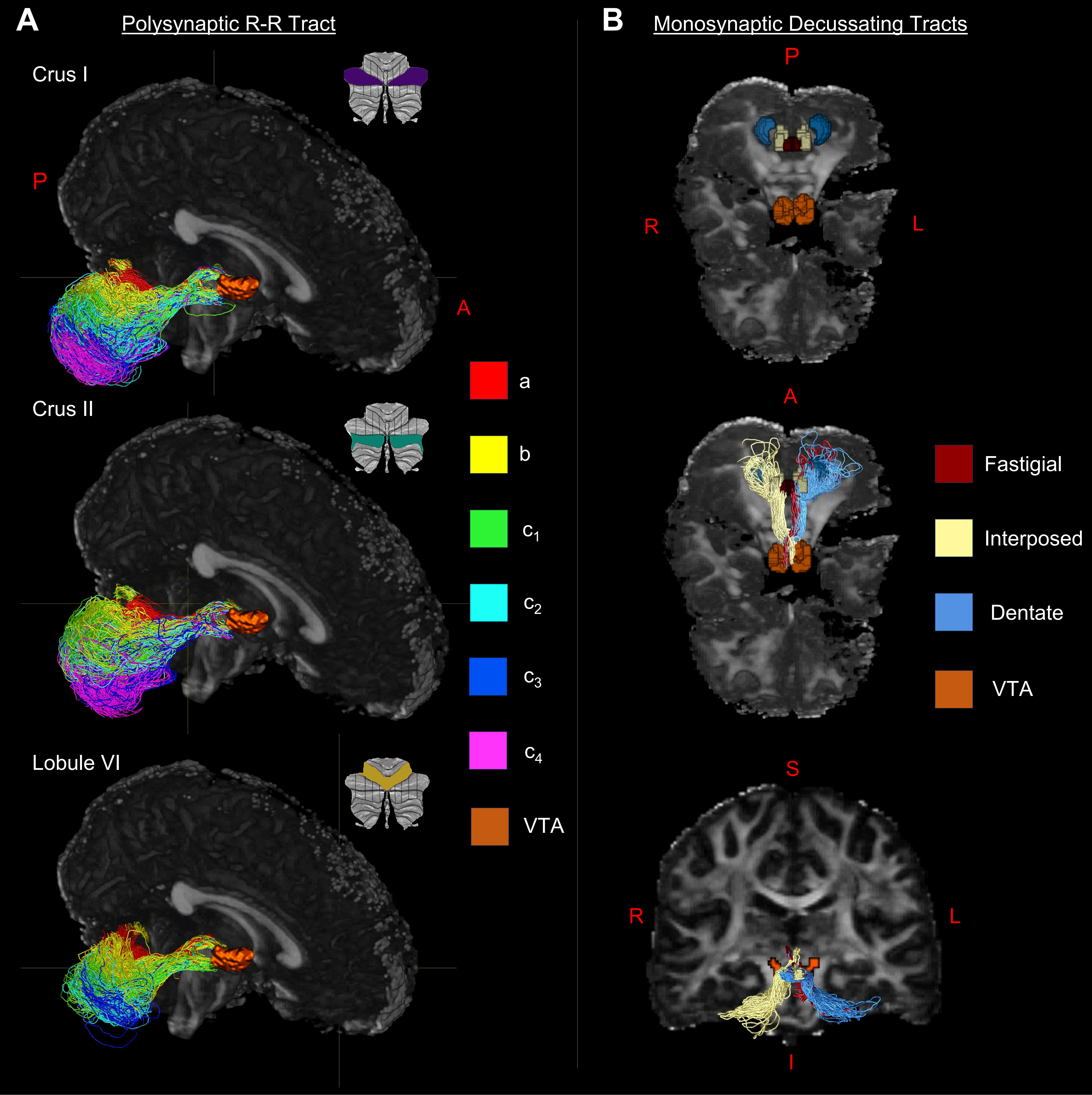
A
Polysynaptic R-R Tract
Crus I
P
A
Crus II
Lobule VI
a
b
c_1
c_2
c_3
c_4
VTA
B
Monosynaptic Decussating Tracts
P
R
L
A
Fastigial
Interposed
Dentate
VTA
S
R
L
I

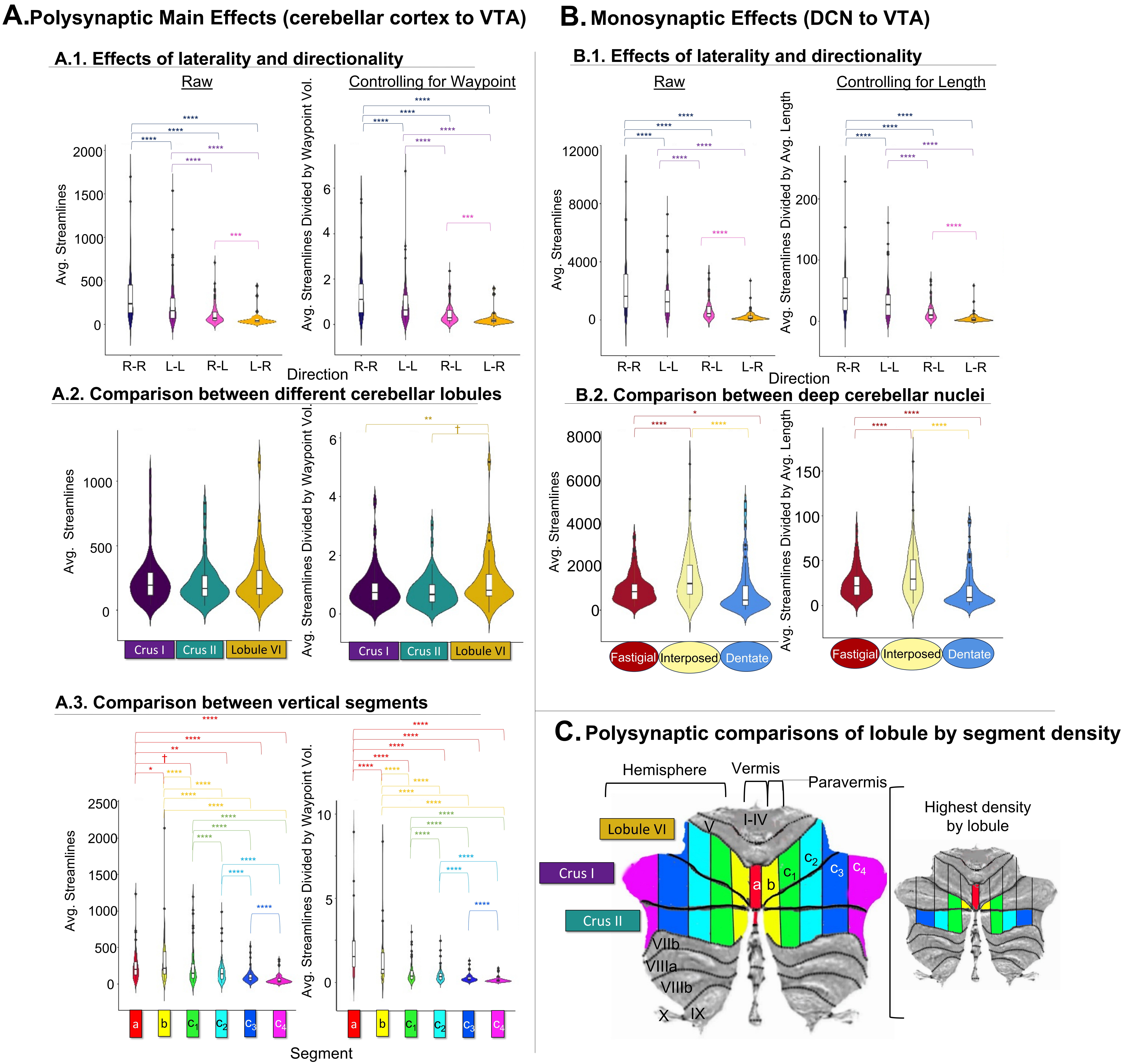
A. Polysynaptic Main Effects (cerebellar cortex to VTA)
A.1. Effects of laterality and directionality
Raw
Controlling for Waypoint
Avg. Streamlines
Avg. Streamlines Divided by Waypoint Vol.
2000
1500
1000
500
0
6
4
2
0
****
***
R-R
L-L
R-L
L-R
Direction
A.2. Comparison between different cerebellar lobules
1000
500
0
6
4
2
0
**
†
Crus I
Crus II
Lobule VI
A.3. Comparison between vertical segments
2500
2000
1500
1000
500
0
10
5
0
****
**
†
*
a
b
c_1
c_2
c_3
c_4
Segment
B. Monosynaptic Effects (DCN to VTA)
B.1. Effects of laterality and directionality
Raw
Controlling for Length
Avg. Streamlines
Avg. Streamlines Divided by Avg. Length
12000
8000
4000
0
200
100
0
****
R-R
L-L
R-L
L-R
Direction
B.2. Comparison between deep cerebellar nuclei
8000
6000
4000
2000
0
150
100
50
0
****
*
Fastigial
Interposed
Dentate
C. Polysynaptic comparisons of lobule by segment density
Hemisphere
Vermis
Paravermis
Lobule VI
Crus I
Crus II
V
I-IV
a
b
c_1
c_2
c_3
c_4
VIIb
VIIIa
VIIIb
X
IX
Highest density by lobule

a. Medial-to-lateral gradient of connectivity within each cerebellar lobule

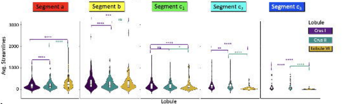

b. Representative tracts of segments with highest connectivity to VTA

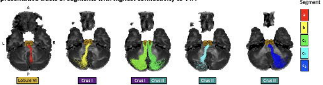
Segment
A
L
R
P
a
b
c_1
c_2
c_3
Lobule VI
Crus I
Crus I
Crus II
Crus II
Crus II

A. Polysynaptic effects of laterality, directionality, lobule, and segment controlling for length

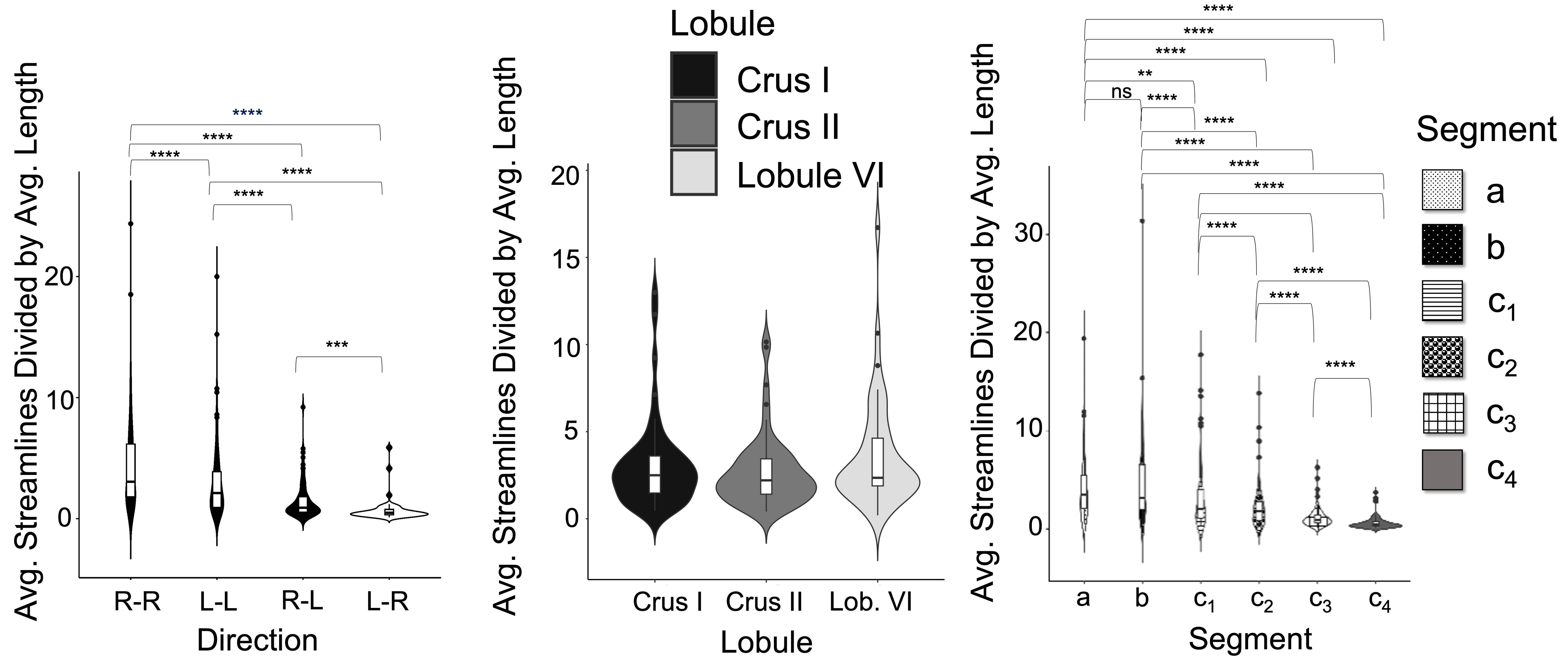

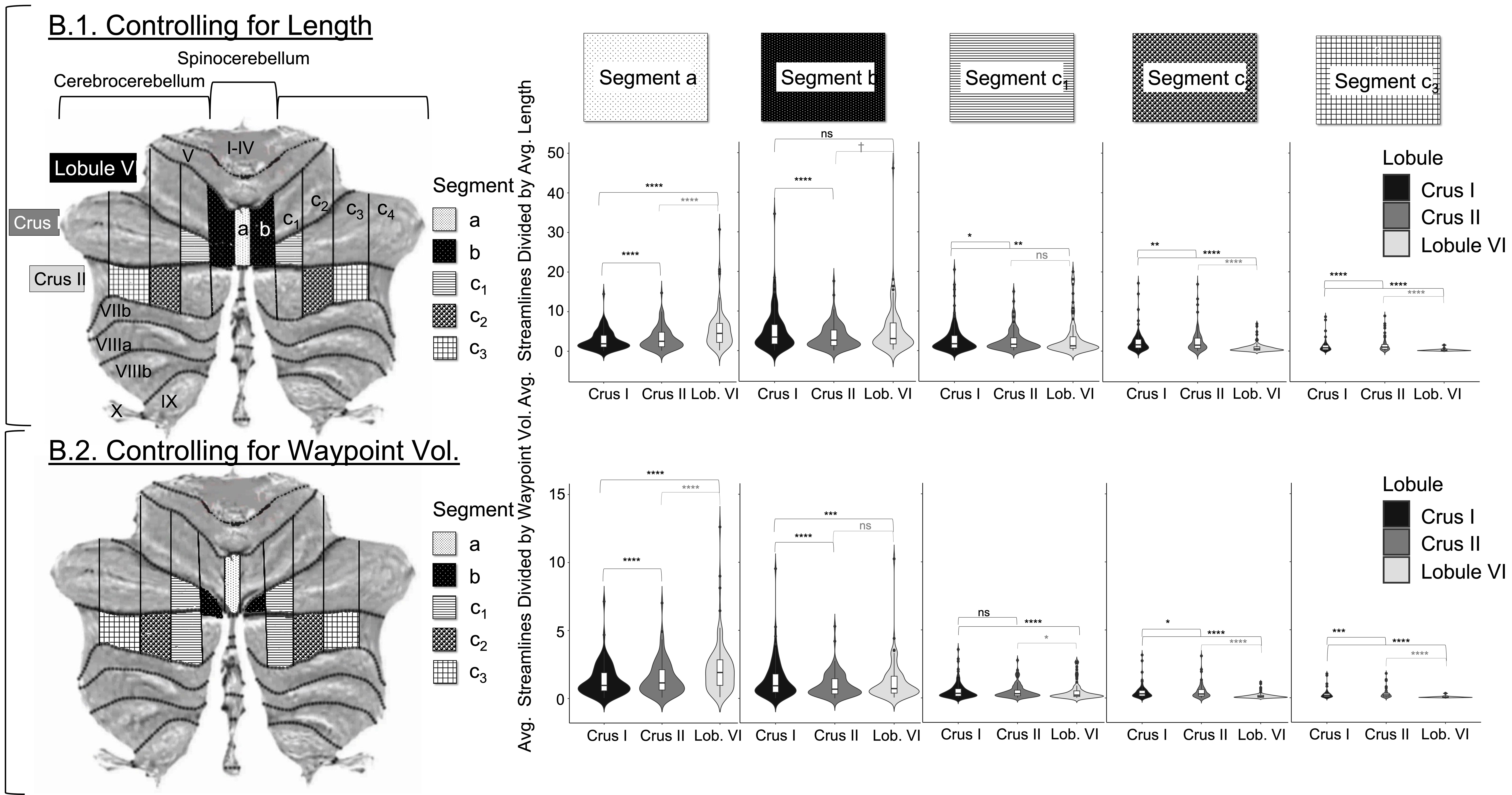B. Polysynaptic comparisons of lobule by segment density with controls